7-2011

Negative Polaron And Triplet Exciton Diffusion In Organometallic "molecular Wires"

Julia M. Keller

Ksenija D. Glusac
Bowling Green State University, kglusac@bgsu.edu

Evgeny O. Danilov

Sean McIlroy

Paiboon Sreearuothai

See next page for additional authors

JACS
JOURNAL OF THE AMERICAN CHEMICAL SOCIETY

ARTICLE

pubs.acs.org/JACS

Negative Polaron and Triplet Exciton Diffusion in Organometallic "Molecular Wires"

Julia M. Keller,[†] Ksenija D. Glusac,[‡] Evgeny O. Danilov,[‡] Sean McIlroy,[§] Paiboon Sreearuothai,[§] Andrew R. Cook,[§] Hui Jiang,[†] John R. Miller,*[,§] and Kirk S. Schanze*[,†]

[†]Department of Chemistry, University of Florida, P.O. Box 117200, Gainesville, Florida 32611, United States

[‡]Department of Chemistry, Bowling Green State University, Bowling Green, Ohio 43403, United States

[§]Chemistry Department, Brookhaven National Laboratory, Upton, New York 11973, United States

Supporting Information

ABSTRACT: The dynamics of negative polaron and triplet exciton transport within a series of monodisperse platinum (Pt) acetylide oligomers is reported. The oligomers consist of Pt−acetylide repeats, $[PtL_2-C\equiv C-Ph-C\equiv C-]_n$ (where L = PBu_3 and Ph = 1,4-phenylene, n = 2, 3, 6, and 10), capped with naphthalene diimide (NDI) end groups. The Pt−acetylide segments are electro- and photoactive, and they serve as conduits for transport of electrons (negative polaron) and triplet excitons. The NDI end groups are relatively strong acceptors, serving as traps for the carriers. Negative polaron transport is studied by using pulse radiolysis/transient absorption at the Brookhaven National Laboratory Laser-Electron Accelerator Facility (LEAF). Electrons are rapidly attached to the oligomers, with some fraction initially residing upon the Pt−acetylide chains. The dynamics of transport are resolved by monitoring the spectral changes associated with transfer of electrons from the chain to the NDI end group. Triplet exciton transport is studied by femtosecond−picosecond transient absorption spectroscopy. Near-UV excitation leads to rapid production of triplet excitons localized on the Pt−acetylide chains. The excitons transport to the chain ends, where they are annihilated by charge separation with the NDI end group. The dynamics of triplet transport are resolved by transient absorption spectroscopy, taking advantage of the changes in spectra associated with decay of the triplet exciton and rise of the charge-separated state. The results indicate that negative polarons and excitons are transported rapidly, on average moving distances of ∼3 nm in less than 200 ps. Analysis of the dynamics suggests diffusive transport by a site-to-site hopping mechanism with hopping times of ∼27 ps for triplets and <10 ps for electrons.

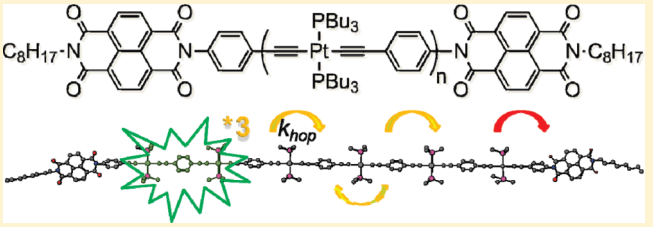

INTRODUCTION

Electron and energy transfer are two of the most significant and fundamental processes in chemistry and biology. For example, the primary events of light harvesting, energy transport, and electron transfer that occur in the photosynthetic apparatus rely on rapid and efficient energy and electron transfer over significant distances.[1−3] The ongoing technology research/development effort in the area of organic electronic devices is in part focused on discovering ways to enhance exciton and charge transport over long distances in organic semiconducting materials. One approach to this problem has been to examine the factors that control transport within or across saturated (insulating) or π-conjugated (conducting or semiconducting) single molecules.[4−10] These constructs have been referred to as "molecular wires",[11−14] and it is hoped that single molecular chains could ultimately be used as interconnects or active elements in molecular electronic devices.[15,16]

Studies of transport within or across single molecular wires (spacers) have primarily focused on transport across π-conjugated organic systems.[17−19] One approach to this problem is to apply fast time-resolved spectroscopy and/or pulse radiolysis to measure the dynamics of photoinduced energy or electron transfer from a donor to an acceptor across an intervening spacer.[19] During the past decade studies have reported exciton and charge transport over very long distances (50−100 nm) in polydisperse π-conjugated polymers that are functionalized with molecular units that serve as traps for the carriers (e.g., low-redox potential electron acceptors serve as traps for electrons).[20,21] Notable studies have applied ultrafast time-scale pump−probe spectroscopy or pulse radiolysis to study singlet exciton and electron transport within long molecular wires consisting of π-conjugated polymer backbones.[21−26] These studies conclude that transport is rapid, yet it is dominated by incoherent hopping of the carriers between segments defined by structural disorder in the π-conjugated system.

While considerable work has been carried out to examine transport in conjugated organic systems, comparatively less is known about transport in conjugated systems that incorporate transition metals. The research community is showing increasing

Received: March 30, 2011
Published: June 06, 2011

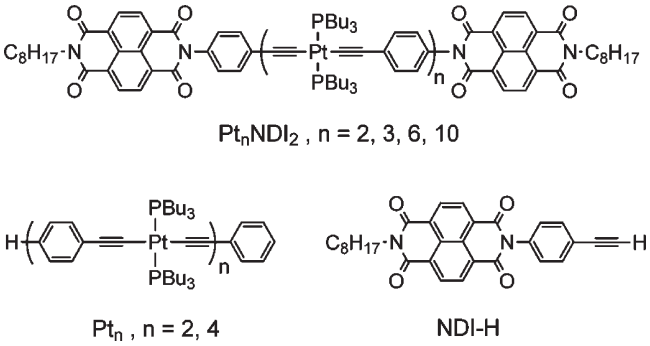

Figure 1. Structural formulas for compounds investigated.

interest in these materials because transition-metal-containing molecules and polymers are essential components in high-efficiency organic light-emitting diodes (LEDs).[27,28] In addition, metal-containing materials are gaining interest for application in bulk heterojunction solar cells.[29,30]

Platinum (Pt) acetylide oligomers and polymers, $[PtL_2-C\equiv C-Ar-C\equiv C-]_n$ (where L = a phosphine ligand and Ar = a π-conjugated arylene unit), are a versatile platform for fundamental studies directed at understanding the effect of heavy metal centers on exciton structure and charge transport in π-conjugated systems.[31−41] In particular, Pt−acetylides are of interest due to their excited state properties which are dominated by long-lived triplet excitons as well as their potential optoelectronic applications including polymer LEDs,[42,43] bulk heterojunction solar cells,[29,30,44] and nonlinear optical materials.[45−47] In the past several years we have explored the optoelectronic properties of platinum Pt−acetylide oligomers and polymers in an effort to define the structure and dynamics of triplet excitons and charge carriers (negative and positive polarons) in organometallic π-conjugated electronic systems.[36−39,48] Results of steady-state and time-resolved spectroscopy and pulse-radiolysis studies indicate that the triplet exciton and negative and positive polaron states in Pt−acetylides are spatially confined to a chromophore segment consisting of one to two repeat units.[39,48] Experimental results and quantum calculations also imply that exciton and charge state delocalization in Pt−acetylides is influenced by the relative conformation of the arylene rings and the square planar PtL_2C_2 units within the backbone.[39,48] Evidence of exciton and polaron diffusion in Pt−acetylide oligomers and polymers has also been reported,[49,50] which brings up questions regarding the mechanism and dynamics of carrier transport in these organometallic conjugated materials.[51]

In the present investigation we expanded on our previous work on Pt−acetylides in an effort to provide definitive results regarding the dynamics of triplet exciton and negative polaron (electron) transport along single "molecular wires" consisting of long monodisperse Pt−acetylide oligomers. As reported recently, we synthesized a series of monodisperse oligomers (Pt_nNDI_2, where n = 2, 3, 6, and 10 shown in Figure 1) end capped with naphthalene diimide (NDI) units that serve as traps for triplet excitons (via charge separation) and negative polarons (by charge shift from the chain to the end group).[52] Here, we report the results of fast time-scale pump−probe spectroscopy and pulse radiolysis experiments on the dynamics of triplet exciton and negative polaron transport along the chains. This work shows that triplet excitons and negative polarons, initially localized on the Pt−acetylide chain, rapidly transport to the chain ends and become trapped by charge separation or charge shift to NDI. The transport rate varies with the length of the Pt−acetylide chain. Analysis of the results suggests that transport occurs via an incoherent hopping mechanism, with triplet excitons moving more slowly (~27 ps per hop) compared to electrons (<10 ps per hop). Transport may be limited in part by electronic coupling terms between adjacent sites on the chain, with the coupling strength larger for electrons compared to triplet excitons. It is also possible that conformational dynamics involving rotation of the arylene units within the conjugated backbone may play a role in determining the hopping dynamics.

MATERIALS AND METHODS

Materials. The synthesis and structural characterization of all molecules used in this study have been previously reported.[36,52] Reagents and solvents were obtained from commercial sources and used as received unless otherwise noted. Tetrahydrofuran was dried by distillation from Na/benzophenone.

Electrochemical and Photophysical Methods. Steady-state absorption spectra were recorded on a Varian Cary 100 dual-beam spectrophotometer. Corrected steady-state emission measurements were conducted on a SPEX F-112 fluorescence spectrometer. Samples were degassed by argon purging for 30 min, and concentrations were adjusted to produce "optically dilute" solutions (i.e., $A_{max} < 0.20$). Photoluminescence quantum yields were determined according to the "optically dilute" method described by Demas and Crosby.[53] Low-temperature luminescence measurements were made by cooling the samples in a LN2-cooled Oxford Instruments Optistat DN-1704 optical cryostat connected to an Omega CYC3200 temperature controller, and emission measurements were conducted on a PTI fluorescence spectrometer. Samples were degassed by four repeated cycles of freeze−pump−thaw on a high-vacuum line.

Cyclic voltammetry (CV) experiments were performed in a dry methylene chloride (CH_2Cl_2) solution containing 0.1 M tetra-*n*-butylammonium hexafluorophosphate (TBAH). The three-electrode setup consisted of a platinum microdisk (2 mm^2) working electrode, a platinum wire auxiliary electrode, and a silver wire reference electrode. Solutions were degassed with argon flow prior to measurements, and positive argon pressure was maintained during the measurements. The concentration of oligomers in the solutions was 1 mM. A 100 mV/s scan rate was used. All potentials were calibrated by using a ferrocene internal standard ($E(Fc/Fc^+) = 0.43$ V vs SCE in CH_2Cl_2), and potentials are reported vs SCE.

Pulse Radiolysis Experiments. This work was carried out at the Brookhaven National Laboratory Laser-Electron Accelerator Facility (LEAF). The LEAF facility and the methods used are described elsewhere,[54−56] as are application to conjugated polymers.[24,57,58] Briefly, the electron pulse (≤50 ps duration) was focused into a quartz cell with an optical path length of 20 or 5 mm containing tetrahydrofuran (THF) solutions under argon. The monitoring light source was a pulsed xenon arc lamp. Wavelengths were selected by using either 40 or 10 nm bandpass interference filters. Transient absorption signals were detected with either silicon or InGaAs photodiodes (EG&G FND-100Q, $\lambda \leq 1000$ nm, and GPD Optoelectronics GAP-500 L, $\lambda \geq 1100$ nm, respectively) or a biplanar phototube (Hamamatsu R1328U-03, $\lambda \leq 650$ nm) and digitized with a LeCroy 8620A-oscilloscope. While most measurements have 2−4 ns time resolution, a 125 ps system rise time was attained in the visible

Table 1. Reaction Scheme for Pulse Radiolysis

reaction	process	entry no.
$RH \rightarrow RH^{\bullet+} + e^-$	solvent ionization	i
$e^- \rightarrow e_s^-$	thermalization, solvation	ii
$RH^{\bullet+} + RH \rightarrow R^\bullet + RH_2^+$	proton transfer	iii
$e_s^- + Pt_nNDI_2 \rightarrow Pt_n^{\bullet-}NDI_2$	e^- attachment to Pt_n chain	a
$e_s^- + Pt_nNDI_2 \rightarrow Pt_nNDI_2^{\bullet-}$	e^- attachment to NDI end group	b
$Pt_n^{\bullet-}NDI_2 + RH_2^+, R^\bullet \rightarrow$ products		c
$e_s^- + RH_2^+, R^\bullet \rightarrow$ products		d
$Pt_n^{\bullet-}NDI_2 \rightarrow Pt_nNDI_2^{\bullet-}$	intramolecular electron transfer	e

using the biplanar phototube along with short path-length cells. An alternative mode used ~7 ps electron pulses and an optical fiber single-shot (OFSS) detection system (see below). Molar extinction coefficients of the radical anions were calculated using G(e-THF) = 0.60 in THF,[59,60] where G is the radiation chemical yield. To account for capture of geminate electrons, many of which decay in times near 1 ns, the yield of anions of a solute took into account the competition between production of anions by electron capture and electron decay using the time-dependent yield of electrons reported by De Waele[60,61] and similar data obtained in this work. Absorbance of the anion of the solute was measured just after electron capture was complete. The extinction coefficients obtained were smaller than those reported earlier for Pt_n ions.[48]

Optical fiber single-shot (OFSS) pulse radiolysis obtains a 15 ps overall time resolution using single electron pulses that are compressed to ~5 ps duration.[62] Signal to noise is enhanced by averaging data from ~25 pulses. Briefly, the system measures transient absorption utilizing laser probe pulses with wavelengths selected by an optical parametric amplifier. Each probe pulse passes through an optical fiber bundle composed of ~100 fibers having different lengths, separating the probe pulse into 100 minipulses having different time delays. The bundle is then imaged into the region of the sample irradiated by the 5 ps electron pulse and then imaged on a CCD array camera. The CCD image is calibrated (fiber "pixel" position vs delay time), and the transient absorption decay trace is recovered from analysis of the calibrated images.

Charge transport to the NDI end caps was analyzed in the reaction scheme shown in Table 1 (see Supporting Information for more detail on the fitting procedure). Fast electrons pass through the sample cell, creating ionization that primarily results in reactive solvated electrons (e_s^-) in THF, abbreviated as RH in the scheme (i and ii), along with solvent cations $RH^{\bullet+}$ that fragment to solvated protons in RH_2^+ and radicals $R^\bullet$ (iii).[63] The electrons are thermalized within a few picoseconds and attach to the oligomers in bimolecular charge transfer reactions (a and b). Neither RH_2^+ or radicals $R^\bullet$ react with the oligomers on the time scales investigated, but both react with radical anions of the oligomers in geminate and homogeneous recombination (c and d). Finally, the reaction of interest is intramolecular electron transfer wherein the electron localized on the chain transfers to an NDI end group (e).

Ultrafast Transient Absorption Spectrometry. Femtosecond time-resolved experiments were performed using the spectrometer available at the Ohio Laboratory for Kinetic Spectroscopy at Bowling Green State University. The laser system output consisted a Ti:Sapphire oscillator/regenerative amplifier as a source of 800 nm light with fwhm of 100 fs operating at a repetition rate of 1 kHz (Hurricane, Spectra Physics). The 800 nm light was split into pump and probe beams. Samples were excited using 352 nm (1 μJ/pulse) light produced using an OPA (Spectra Physics). A white light continuum probe beam was produced using a CaF_2 crystal. Additional details of the experimental parameters have been cited elsewhere.[64]

Random-Walk Numerical Simulation. To simulate the one-dimensional random-walk process numerically, a program was written with Visual Basic in SigmaPlot. Briefly, the oligomer chain length (defined as m, not including the trap sites on both ends) and the desired number of program repetitions (n) are input as simulation parameters. (In the simulations for the Pt_nNDI_2 series $m = n + 1$.) The initial position of the exciton is randomly selected along the oligomer chain by generating a random integer representing where the exciton is initially created, *IniPos* ($1 \leq IniPos \leq m$). If *IniPos* is in the middle of the chain ($1 < IniPos < m$), another random number between 0 and 1 is generated. If this number is in the range between 0.5 and 1, *IniPos* is incremented right (*IniPos* + 1). Otherwise, it is incremented left (*IniPos* − 1). In either case, the counter for the number of random-walk steps taken (*Steps*) is increased by 1 (*Steps* + 1). When *IniPos* reaches a chain end (*IniPos* = 1 or *IniPos* = m), the random-walk stops and the counter for the number of steps taken (*Steps*) is recorded. The same procedure is repeated for the desired number of repetition times (n), and the obtained number of random-walk steps (Steps) are subjected to histogram analysis (*Bin Width* = 5).

RESULTS AND DISCUSSION

Oligomer Structures, Reaction Schemes, and Energetics. The Pt_nNDI_2 series (Figure 1) was selected for this study for several reasons. First, it is formally π-conjugated, with the platinum centers providing electronic communication between adjacent phenylene−ethynylene units via dπ(Pt)/pπ(C) orbital overlap.[65] Second, in previous work we developed an iterative synthetic method involving orthogonal protecting groups allowing synthesis of monodisperse Pt−acetylide oligomers in comparatively high yield.[36] Finally, we and others have characterized the properties of the one-electron reduced and electronic excited states for Pt−acetylide systems in detail.[39,48] This work showed that the negative polaron and triplet exciton states of the Pt−acetylide chain (i.e., $[-Pt(PR_3)_2-C\equiv C-Ph-C\equiv C-]^{\bullet-}{}_n$ and $^3[-Pt(PR_3)_2-C\equiv C-Ph-C\equiv C-]^*{}_n$, respectively) are concentrated on a relatively short oligomer segment consisting of just over a single repeat unit. Because of this localization, we anticipated that transport along a Pt−acetylide segment will occur by a sequence of electron or exciton "hops" between

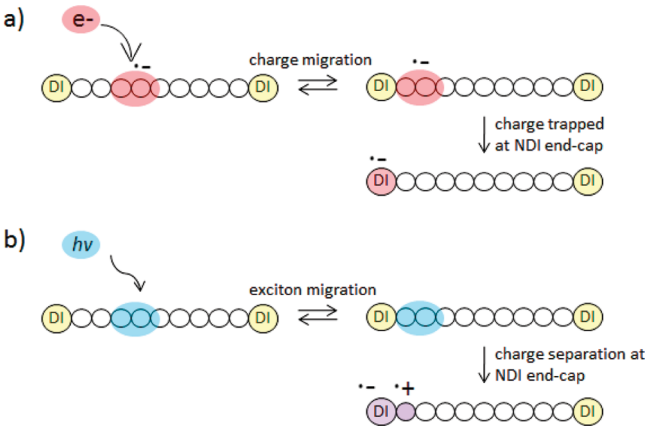

Figure 2. Schematic of electron (a) and exciton (b) transport in Pt_nNDI_2 oligomers. DI represents the naphthalene diimide end-group trap.

adjacent repeat units. The NDI end group was selected as a "trap" for the negative polaron and triplet exciton states because it undergoes one-electron reduction at a comparatively low potential and the spectral signature of the anion state, $NDI^{\bullet -}$, is distinct and can be distinguished by visible-region transient absorption spectroscopy.[66] Model compounds (Pt_2, Pt_4, and NDI−H, Figure 1) were used to provide reference data (transient absorption spectra and kinetics) needed for analysis of the electron and exciton transport dynamics.

Figure 2 shows schematic diagrams illustrating the general concepts for negative polaron and triplet exciton transport in the Pt_nNDI_2 oligomers. Polaron transport dynamics are investigated by using pulse radiolysis, Figure 2a. Electrons produced by pulse radiolysis attach to the Pt_nNDI_2 oligomers in a diffusion-controlled reaction, affording negative polaron states distributed nearly randomly along a Pt−acetylide chain (as well as on the NDI end groups). The location of the electron (Pt−acetylide chain vs NDI end group) is determined by using wavelength and time-resolved transient absorption spectroscopy, taking advantage of the differences in the visible absorption spectra of the Pt−acetylide chain polaron and NDI-localized radical anion states. The dynamics of electron transport from the Pt−acetylide chain to an NDI end group are monitored by time-resolved absorption at selected wavelengths.

Triplet exciton transport is studied by picosecond time-resolved absorption spectroscopy, Figure 2b. Optical pulse excitation produces a singlet exciton on the Pt−acetylide chain; the singlet undergoes rapid (<5 ps) intersystem crossing to produce a triplet exciton state.[67] The triplet exciton then undergoes transport to a chain end, where it is quenched by electron transfer, affording a charge-separated state which subsequently decays by charge recombination. Triplet exciton transport is monitored by transient absorption spectroscopy, taking advantage of the difference in visible absorption spectra of the triplet exciton and charge-separated states.

Optical spectroscopy and electrochemistry provide information regarding relative energies of the various states involved in the processes outlined in Figure 2. In particular, the energies of the singlet and triplet exciton states for the Pt−acetylide chain are available from fluorescence and phosphoresence spectra. The reduction and oxidation potentials for the NDI unit and the Pt−aceylide chain are available from cyclic voltammetry, and the

Table 2. Table of Energetics

oligomer	$E_{singlet}$ /eV	$E_{triplet}$ /eV	E_{red}/V[a]	E_{ox} /V[a]	E_{CS} /V[b]
Pt_2[c]	3.32	2.40	−1.27	0.89	
Pt_4[c]	3.19	2.39	−1.30	0.89/0.88	
Pt_2NDI_2[d]	3.12	2.41	−0.65	0.89	1.35
NDI−H	3.21	2.04	−0.53[66]		

[a] Potential reported versus SCE. [b] $E_{CS} = E_{ox} - E_{red} - 14.4/\varepsilon R_{DA}$.[68] [c] From ref 48. [d] From ref 52.

energy of the charge-separated state is estimated from the difference in the Pt−acetylide chain oxidation and NDI reduction potentials. Table 2 collects the values for these parameters as determined from studies of the model compounds (Pt_2, Pt_4, and NDI−H) and Pt_2NDI_2. First, examining the electrochemistry data, it is seen that the Pt−acetylide chain exhibits a reduction at ca. −1.3 V and an oxidation at +0.89 V, whereas the NDI unit features a reduction at −0.65 (in Pt_2NDI_2).

From these data we conclude that the electron transfer reaction from the Pt−acetylide negative polaron state producing the NDI radical anion is moderately exothermic with $\Delta G \approx -0.65$ eV ($\Delta G \approx -1.3$ eV + 0.65 eV)

$$\begin{aligned} &NDI{-}[-PtL_2{-}C{\equiv}C{-}Ph{-}C{\equiv}C{-}]_n^{\bullet -}{-}NDI \rightarrow \\ &NDI{-}[-PtL_2{-}C{\equiv}C{-}Ph{-}C{\equiv}C{-}]_n{-}NDI^{\bullet -} \end{aligned} \quad (1)$$

Next, by taking the energy of the Pt−acetylide triplet exciton (~2.40 eV) and the energy of the charge-separated state ($E_{cs} \approx$ 1.35 eV), it is seen that the triplet exciton quenching reaction is strongly exothermic with $\Delta G \approx -1.05$ eV ($\Delta G \approx 1.35-2.40$ eV):[69]

$$\begin{aligned} &NDI{-}{}^3[-PtL_2{-}C{\equiv}C{-}Ph{-}C{\equiv}C{-}]_n{*}{-}NDI \rightarrow \\ &NDI{-}[-PtL_2{-}C{\equiv}C{-}Ph{-}C{\equiv}C{-}]_n^{\bullet +}{-}NDI^{\bullet -} \end{aligned} \quad (2)$$

This analysis shows that the steps in Figure 2a and 2b leading to polaron or triplet exciton trapping by NDI are moderately to strongly exothermic and thus are unlikely to be overall rate-determining steps for triplet exciton quenching. This point is discussed in greater detail below. Note that the charge-separated state is certain to be strongly bound by Coulomb attraction and is unlikely to separate within its lifetime.

Pulse Radiolysis and Negative Polaron Transport. Pulse radiolysis was carried out on THF solutions of the NDI end-capped oligomers (Pt_nNDI_2) and model compounds Pt_4 and NDI−H. As described in the Methods section and detailed in Table 1, electron beam irradiation in THF rapidly produces solvated electrons (e_s^-) which serve as a promiscuous reducing agent, rapidly generating negative polaron states of the oligomers. Initial electron attachment is expected to be nearly random, resulting in a distribution of chain-localized and NDI end-group anion states. The electron attachment (reduction) reaction is pseudo-first order in the (oligomer) substrate, and therefore, in order to decrease the time scale of the reduction reaction pulse radiolysis was carried out at relatively high oligomer concentration.

Figure 3a compares visible region transient absorption spectra for radical anions of Pt_4, NDI−H, and $Pt_{10}NDI_2$ observed ~20 ns following pulse radiolysis in THF solution. The spectra also feature weak near-infrared bands, as shown in an extended version of the plot (Figure S1) in the Supporting Information. The absorption spectra of the radical anions of Pt_2NDI_2 and Pt_6NDI_2, shown in Figure S2 (Supporting Information), are

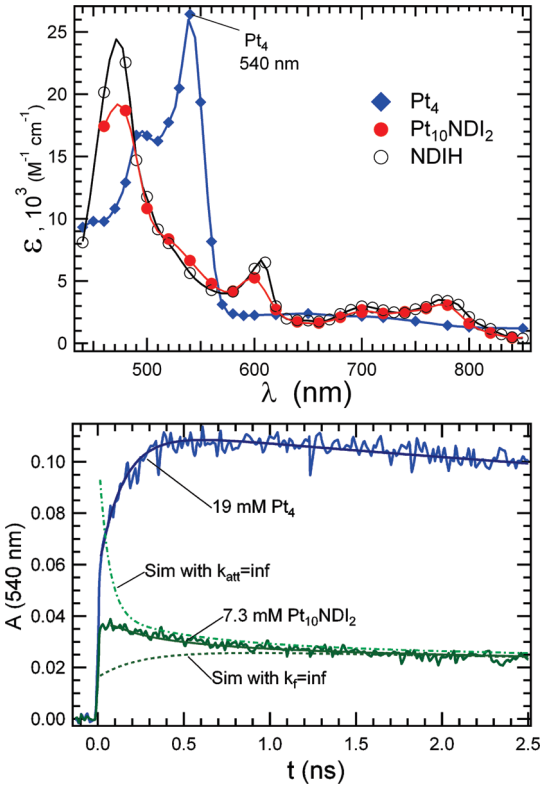

Figure 3. (a) Transient absorption spectra of $Pt_4^{\bullet-}$, $Pt_{10}NDI_2^{\bullet-}$, and $NDIH^{\bullet-}$ ~20 ns after pulse radiolysis in THF. (b) Transient absorption at 540 nm of 7.3 mM $Pt_{10}NDI_2$ in THF compared with that for 19 mM Pt_4 in THF. Fits with the kinetic model in Table 1 are shown passing through the data. The fits indicate that 38% of electrons attached to $Pt_{10}NDI_2$ are captured immediately (≪15 ps) on the NDI traps. The remaining 62% of the electrons appear in the Pt chains and transport to and are captured by the NDI end traps with two rates with $1/k_f$ = 59 ps (0.53) and 660 ps (0.09). The broken lines in the plot are simulated curves calculated by the fitting function with both components of k_f set to infinity (k_f corresponds to process e in Table 1) or with k_f set to the fit value but with infinitely fast e^- capture (k_{att} = infinity; this corresponds to process a in Table 1).

similar to that for $Pt_{10}NDI_2$ and the isolated end-cap anion NDI−H. With the exception of Pt_4, the spectra of all of the anion radicals are the same with $\lambda_{max} \approx 475$ nm and weaker bands at 610, 700, and 780 nm; this is consistent with the spectrum of the naphthalene diimide radical anion, $NDI^{\bullet-}$.[66] The spectrum observed for Pt_4 features a prominent absorption with $\lambda_{max} \approx$ 540 nm, and the spectrum is the same as that reported in our earlier study,[48] where the band was assigned to the Pt−acetylide chain-localized negative polaron, $-(PtL_2-C\equiv C-Ph-C\equiv C-)_n^{\bullet-}$. The important conclusion that can be made on the basis of the transient absorption spectra is that electrons attached to Pt_2NDI_2, Pt_6NDI_2, and $Pt_{10}NDI_2$ appear rapidly (t < 20 ns) on the NDI groups. From this we can infer that even in the long oligomers Pt_6NDI_2 and $Pt_{10}NDI_2$ transport of the polaron to the NDI end groups is rapid, occurring on a time scale faster than is accessible on the conventional pulse radiolysis system used for the transient absorption spectral studies (rise time ≈ 2 ns, $k > 5 \times 10^8$ s^{-1}).

Using the OFSS pulse radiolysis system, which has significantly improved time resolution (rise time ≈ 15 ps), we reexamined the fast-time-scale dynamics of the $Pt_{10}NDI_2$ oligomer negative polaron state. As can be seen in Figure 3a, the absorption spectrum of the chain-localized polaron exhibits a maximum at 540 nm whereas the NDI-localized radical anion absorbs at shorter wavelength (475 nm). Thus, by monitoring the transient absorption at 540 nm with the OFSS it is possible to monitor the dynamics of the chain-localized polaron state, with little interference from the NDI radical anion state. Figure 3b compares the OFSS transient absorption dynamics at 540 nm for Pt_4 (c = 19 mM) and $Pt_{10}NDI_2$ (c = 7.3 mM) in THF solution. This data reveals that Pt_4 anions are produced in a prompt component (τ < 20 ps) followed by an additional 160 ps component which is due to attachment of solvated electrons. The prompt rise component is due to capture of electrons before they are solvated (i.e., prior to reaction ii in Table 1).[70] The efficiency of this prompt capture of unsolvated or "dry electrons" was recently found to be proportional to the chain length of a polymer or an oligomer,[70] making Pt_4 a good reference for $Pt_{10}NDI_2$ when used at a concentration almost three times larger.

Interestingly, as can be seen in Figure 3b, the transient absorption profile at 540 nm for $Pt_{10}NDI_2$ is distinctly different compared to that of the Pt_4 reference. In particular, the absorption exhibits only a prompt rise component and then a small amplitude decay occurs over a 500 ps time scale. The final transient absorption amplitude is ~4 times less than that of Pt_4, consistent with the weaker absorptivity of the $NDI^{\bullet-}$ state at 540 nm compared to that of the Pt−acetylide negative polaron. Importantly, the transient absorption dynamics of the $Pt_{10}NDI_2$ anion at 540 nm do not feature a slow rise as observed for the Pt_4 model. Qualitatively this difference in the dynamics arises because the observed transient absorption consists of the superposition of absorption decay (due to electron transfer from the Pt−acetylide chain to the NDI end group) onto absorption rise that occurs due to attachment of solvated electrons. This notion is illustrated by the simulations shown as broken lines in Figure 3b, where the transient absorption dynamics are simulated under the assumption that (1) electron attachment to the Pt−acetylide chain is instantaneous (k_{att} = inf, Figure 3b) or (2) transport of the polaron from the chain to the NDI end groups is instantaneous (k_f = inf, Figure 3b). The OFSS instrument is not presently capable of observations at 480 nm, but rough indications of the rise of $NDI^{\bullet-}$ are shown in Figure S3, Supporting Information.[71]

In order to extract quantitative information from the $Pt_{10}NDI_2$ anion transient absorption dynamics, the OFSS data in Figure 3b was fitted using the reactions listed in Table 1. The fit results indicate that electron transport from the Pt−acetylide chain to the NDI end groups occurs with biexponential kinetics, 59 (53%) and 660 ps (9%), where the fractions (parenthesized) refer to the total number of electrons attached to $Pt_{10}NDI_2$. These are uncertain by ±30% because electron transport occurs simultaneously with electron attachment. The fit curve giving these rates is seen passing through the experimental data in Figure 3b. The results indicate that a substantial fraction, 38%, of electrons attached to $Pt_{10}NDI_2$ are captured immediately (≪ 15 ps) by the NDI trap groups. The NDI trap groups are similar in size to one repeat unit of the Pt chain, so $Pt_{10}NDI_2$ can be considered to comprise 12 units. If we assume that each of these 12 units captures electrons with equal probability, then the observed 38% immediate capture corresponds to electrons attached directly on the NDI groups and the first 1.3 Pt units adjacent to NDI. We conclude that if a negative polaron is produced within 1.3 repeat units of an NDI end group, it transfers immediately to the NDI. Those polarons formed in the central 7.4 units of the chain are

observed as $-(PtL_2-C\equiv C-Ph-C\equiv C-)_n^{\bullet-}$ that must be transported along the chain to react with the NDI end group, and the dynamics of the transport for the ensemble of polaron states is reflected by the biexponential decay that is resolved from the fit analysis. A more detailed discussion of the significance of this result is provided below.

Photophysics and Triplet Exciton Transport. The absorption spectra of the Pt_nNDI_2 complexes are dominated by the allowed π,π^* transitions arising from the Pt−acetylide segment at $\lambda_{max} \approx 350$ nm.[52] Thus, photoexcitation of the oligomers in the near-UV region produces a singlet exciton which, due to strong spin−orbit coupling induced by the platinum centers, rapidly undergoes intersystem crossing to afford a triplet exciton localized on the Pt−acetylide chain.[67] The present work indicates that this occurs in $\tau \approx 1$ ps. Due to its confinement to a single repeat unit[38] we envisioned that in the longer oligomers (Pt_6NDI_2 and $Pt_{10}DNI_2$) triplet quenching would require a series of exciton hopping steps whereby the exciton reaches the end of the chain and is annihilated by charge separation (eq 2 and Figure 2b).

Initial information regarding the mechanism of triplet exciton quenching in the Pt_nNDI_2 oligomers comes from the study of the phosphorescence spectra at ambient and cryogenic temperatures. Platinum acetylide oligomers typically exhibit moderately efficient phosphorescence from the $^3\pi,\pi^*$ exciton. For example, at room temperature in THF solution Pt_4 exhibits a structured phosphorescence band with $\lambda_{max} = 519$ nm and a quantum yield of 7%.[36] By contrast, the phosphorescence emission of all of the Pt−NDI_2 oligomers is strongly quenched, with quantum yields of $\sim 10^{-3}$ observed for room-temperature THF solutions. This efficient phosphorescence quenching is attributed to nonradiative decay via electron transfer quenching of the triplet exciton by the NDI end groups (eq 2 and Figure 2b).

In order to provide further information regarding the mechanism of the luminescence quenching, phosphorescence spectra of the Pt_nNDI_2 series were measured as a function of temperature over the range 80−200 K in deoxygenated 2-methyltetrahydrofuran (MTHF) solution. This liquid is a rigid glass at temperatures below 130 K, and in the region between 130 and 140 K it undergoes a glass-to-fluid transition. The variable-temperature spectra for Pt_nNDI_2 and NDI−H are shown in Figure S4 (Supporting Information). For the shorter oligomers, Pt_2NDI_2 and Pt_3NDI_2, there is little change in the phosphorescence until $T < 100$ K, where weak phosphorescence from the NDI end groups is observed ($\lambda \approx 605$ and 670 nm). However, by contrast, for the longer oligomers Pt_6NDI and $Pt_{10}NDI_2$, for temperatures below the MTHF glass temperature (140 K), the Pt−acetylide phosphorescence emission becomes very efficient ($\lambda_{em} \approx$ 520 nm). The absence of Pt−acetylide phosphorescence in the shorter oligomers in the MTHF glass strongly suggests that electron transfer quenching remains active in these systems at low temperature. This result is unsurprising, given that electron transfer is strongly exothermic (eq 2).[72] Importantly, the appearance of strong Pt−acetylide phosphorescence for the longer oligomers in the low-temperature glass indicates that exciton transport to the chain ends is slow in the rigid matrix.

Transient absorption spectroscopy was applied to monitor the dynamics of exciton transport and charge separation in the Pt_nNDI_2 series at ambient temperature (Figures 4 and 5). Focusing first on the spectra of the short oligomers (Pt_2NDI_2 and Pt_3NDI_2, Figure 4) it can be seen that very soon after excitation ($t < 15$ ps) the spectra are dominated by a strong

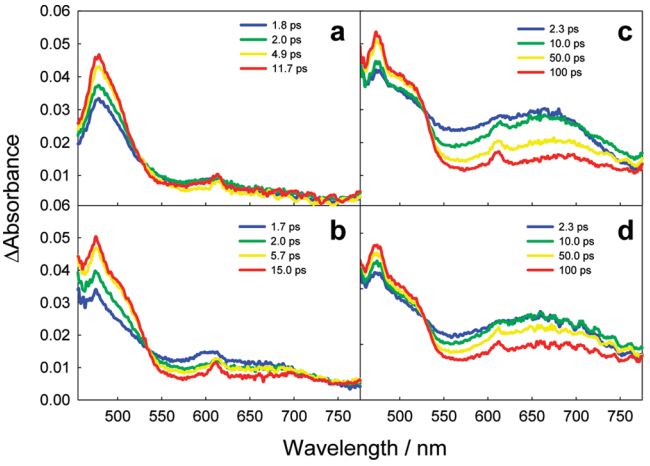

Figure 4. Transient absorption spectra for Pt_nNDI_2 complexes obtained following 100 fs, 352 nm excitation: (a) $n = 2$, (b) $n = 3$, (c) $n = 6$, (d) $n = 10$. Delay times are shown in the insets.

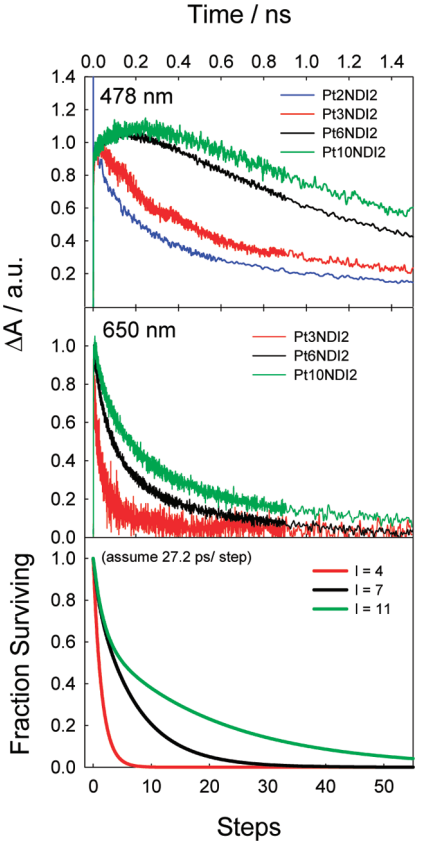

Figure 5. Plot of the normalized transient absorption kinetic traces of the Pt_nNDI_2 series at 478 (top) and 650 nm (middle), and random-walk simulation of the triplet exciton decay profile (bottom). Simulation results placed on time axis by assuming 27.2 ps per step.

absorption with $\lambda_{max} \approx 480$ nm and weak absorption in the rest of the visible region with a small peak at $\lambda_{max} \approx 610$ nm. These prominent bands are due to the naphthalene diimide radical anion, $NDI^{\bullet-}$, that is present in the charge-separated state that is produced by electron transfer (eq 2).[66] Note that in the spectrum of Pt_3NDI_2 the strong band in the blue region has a distinct shoulder at

$\lambda \approx 500$ nm (this feature is also present in the spectra of Pt_6NDI and $Pt_{10}NDI_2$). This feature is attributed to the Pt−acetylide chain-localized positive polaron, $[-PtL_2-C\equiv C-Ph-C\equiv C-PtL_2-]^{\bullet+}$, that is present in the charge-separated state.[48] Taken together, the transient absorption spectral data for Pt_2NDI_2 and Pt_3NDI_2 indicate that the charge-separated state is produced quickly after near-UV excitation.

Turning now to the time-resolved spectra for the longer oligomers Pt_6NDI and $Pt_{10}NDI_2$, it can be seen that the temporal evolution in the spectra occurs more slowly. At early times the spectra feature a broad absorption in the red with at $\lambda_{max} \approx$ 650 nm. With increasing delay time this band decays and the spectrum evolves into the bands characteristic of the charge-separated state. The broad band in the red that is present in the early time spectra is due to the Pt−acetylide localized triplet exciton,[39] and the temporal evolution of the spectra reveals the dynamics of triplet exciton diffusion to the chain ends and charge separation.

Detailed insight concerning the exciton transport dynamics comes from consideration of the transient absorption kinetics at specific wavelengths (Figure 5). In particular, when monitoring at 478 nm (Figure 5, top), the signal is dominated by the $NDI^{\bullet-}$ absorption; thus, this wavelength primarily probes the charge-separated state. By contrast, the signal at 650 nm (Figure 5, middle) is dominated by the absorption of the Pt−acetylide triplet exciton. Interestingly, the absorption at 478 nm for Pt_3NDI, Pt_6NDI, and $Pt_{10}NDI_2$ increases at early delay times, and the rate of the absorption increase slows with increasing oligomer length. The absorption increase is due to formation of the charge-separated state, and the oligomer length dependence reflects the difference in time scale for triplet exciton diffusion along the Pt−acetylide chains.[73]

The transient absorption kinetics at 650 nm exhibit only a decay, with the decay time increasing with oligomer length. At this wavelength the absorption is due only to the triplet exciton, so these kinetic traces provide direct insight regarding the dynamics of triplet exciton diffusion and decay via charge separation. Analysis of the 650 nm decays reveals that they are nonexponential; a biexponential fit affords median lifetimes of 8.3, 203, and 373 ps for Pt_3NDI, Pt_6NDI, and $Pt_{10}NDI_2$, respectively. The fact that the decays are nonexponential is consistent with a model in which the kinetics reflect an inhomogeneous distribution of excited oligomers where the triplet excitons are initially created randomly along the chain. Excitons that are created near the end groups decay rapidly, whereas those that are created near the middle of the chain decay more slowly as they must diffuse to the chain end before undergoing charge separation. A quantitative dynamics model for the transport is discussed below.

Mechanism and Dynamics of Polaron and Exciton Transport. As discussed above, optical data obtained from previous pulse radiolysis studies of Pt_n oligomers reveal that the polaron state is spatially confined.[48] Specifically, the spectrum of the negative polaron state for each member of the series ($Pt_n^{\bullet-}$) displays a characteristic maximum absorption at 540 nm, and the spectra are essentially the same for the series ranging from Pt_2 to Pt_5. Similarly, photophysical studies reveal that the triplet exciton in the Pt_n series is spatially concentrated; this conclusion was based on similar $^3\pi,\pi^*$ phosphorescence emission energies (ca. 520 nm) throughout the series as well as very similar triplet−triplet absorption energies (ca. 650 nm) regardless of oligomer length.[36] For both the triplet and the negative polaron the state is concentrated on a repeat segment that is approximated by the structure $[-PtL_2-C\equiv C-Ph-C\equiv C-PtL_2-]$.

Spatial confinement of these states occurs due to lattice polarization or structural deformations within the oligomer backbone that disrupt conjugation along the chain. Density functional calculations of both the triplet exciton and the negative polaron of Pt_2 revealed significant differences in the minimum energy geometry between the ground state species and the exciton or polaron states that contribute to the localization of these states.[39,48] Specifically, the lowest energy geometry of the ground state exists with all phenyl groups of Pt_2 lying in a plane that is perpendicular to the plane defined by the square planar platinum complex; by contrast, the minimum energy geometry of the negative polaron state was calculated with all phenyl moieties parallel to this plane. The calculated barrier to rotation of the phenyl ring in the radical anion species was estimated to be ~15 kcal/mol. The calculated energy minimum conformation for the triplet exciton exists with only the center phenylene unit in the plane; in the triplet state the barrier to rotation of the central phenylene unit was estimated to be ~3.1 kcal/mol.[39] Compare this to the ground state barrier to phenylene rotation, calculated as 0.5−0.8 kcal/mol.[39] Taken together, the results of these computational and spectroscopic studies support the notion that the negative polaron and triplet exciton states are confined by structural distortions in the platinum acetylide chain. Although quantitative data is not available, on the basis of the photophysical evidence and the calculation results we estimate that the reorganization energy associated with the localization is in the range 2−5 kcal/mol.

We now turn to consider the mechanism for transport of the exciton and polaron states along the platinum acetylide chain. Given that these states are spatially confined, transport along the chain must occur by a site-to-site hopping process. Specifically, a state moves in random directions to adjacent locations on the chain, generating a diffusion ending at the end-group trap (Figure 6). The transitions that constitute diffusive steps along the chain or transfer from the chain to the trap require electronic couplings and nuclear overlap. Electronic couplings can arise from dipole−dipole (Förster resonance energy transfer, FRET) and/or exchange interactions. FRET does not apply to transfer of electrons, and dipole−dipole coupling is negligible for triplet excitons. Thus, for experiments on electrons and triplets in the chains, only one- and two-electron exchange interactions are important. These interactions fall exponentially with distance, giving rates that decrease by a factor of 10 for each 1−3 Å change in distance, with the coupling falling more rapidly with distance for energy transfer.[10,74] For this reason, we believe that the dominant mechanism is diffusive transport (hopping between adjacent sites) until the state arrives at one end of the chain. As depicted in Figure 6, the final step is electron transfer to the trap (or charge separation) when the electron or exciton has reached a point sufficiently close (probably just a few Angstroms) from the chain end. This "chain-end" polaron or exciton state may actually contact the end of the conjugated chain or might be slightly farther from the trap as depicted in the figure.

Designating the overall rate of diffusional transport toward the chain end as k_1, diffusion away from the end as k_{-1}, and transfer from the chain end to the trap as k_2, we have the following kinetics scheme

$$P_c \underset{k_{-1}}{\overset{k_1}{\rightleftharpoons}} P_e \xrightarrow{k_2} T \qquad (3)$$

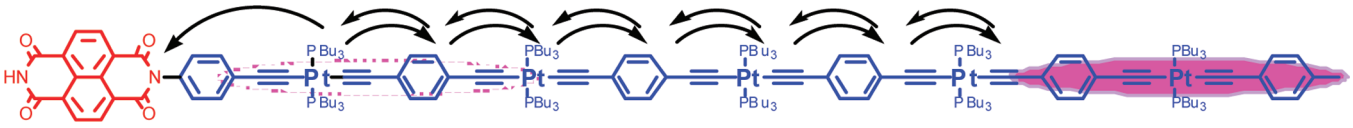

Figure 6. Polaron or exciton diffusion via a random hopping mechanism. One-half (5 units) of a $Pt_{10}NDI_2$ molecule is shown. A polaron or an exciton concentrated on ~1.5 repeat units near the middle of the chain is depicted as a solid magenta ellipse at the right. Diffusion of the polaron to a location near the NDI end-group trap (dashed ellipse) is followed by rapid transfer to the NDI trap.

where the symbols designate a charge or exciton in the Pt—acetylide chain (P_c), at the chain end (P_e), or on the trap (T). In the limit $k_2 \gg k_1$ (transport is rate determining) the observed rate of exciton or polaron transfer to the trap is equal to k_1. Note that that diffusional transport rate, k_1, is not a single rate; here, we model the rate using a numerical simulation for a random-walk process on a one-dimensional ladder as described in the Experimental Section. In this treatment, k_{-1} is not a separate rate but is inherent in the random walk.

Figure 5c shows the random-walk simulation results for triplet exciton decay in Pt_nNDI_2 oligomers with n = 3, 6, or 10. These histograms are placed on a time scale for comparison with the experimental exciton decay kinetics (Figure 5b) by assuming a hopping step time of 27.2 ps. As shown in the figure, the simulation reproduces the experimental data relatively well. The random-walk simulation results are also compared to the negative polaron transport dynamics for $Pt_{10}NDI_2$. In this case, we compare the transport dynamics that were extracted by modeling the observed kinetic data in Figure 3 as a biexponential decay. As shown in Figure S-5 (Supporting Information) the simulation using the random-walk model does not quantitatively account for the dynamics; however, assuming the model it is evident that the polaron hopping time is <10 ps, which is considerably faster than that for the triplet exciton.

As noted above, the dynamics of exciton and polaron hopping along the Pt—acetylide chain are governed by electronic coupling between adjacent sites and fluctuations in geometry (conformational dynamics).[75,76] The fact that polaron transport is faster than triplet exciton transport suggests that site-to-site electronic coupling for electron transfer is larger than for triplet (exchange) transfer. However, it is also interesting to note that the triplet exciton step time of 27 ps corresponds reasonably well to the correlation time for phenylene ring torsion in phenylene ethynylene oligomers.[77] This correspondence suggests the possibility that the transport dynamics are influenced or controlled by geometric change(s) that occur within the Pt—acetylide chain that modulate electronic couplings between adjacent segments (e.g., conformational gating).[78]

It is also of interest to compare the observed polaron and exciton transport rates in the Pt—acetylides with related work on transport in π-conjugated polymers. In order to make these comparisons, we use the triplet hopping time (27 ps) and the major decay component for the negative polaron (59 ps) to estimate the diffusion coefficient (D) for the triplet exciton and mobility (μ) for the polaron. In a one-dimensional hopping model the carrier mobility is $\mu = \lambda^2 e/2k_B T\tau$, where τ is the average time for a hop of length λ, e is the electron charge, k_B is the Boltzmann constant, and T is temperature.[79] The diffusion coefficient is therefore $D = \lambda^2/2\tau$. For the triplet exciton with a hop size of one Pt—acetylide repeat unit (~1 nm) taking τ = 27.2 ps this expression gives $D = 1.8 \times 10^{-4}$ cm^2/s. This estimated diffusivity value is several orders of magnitude larger than triplet exciton diffusivity for molecular triplets in (disorderd) glassy solids, which fall in the range 10^{-8}—10^{-6} cm^2/s.[80,81] The larger value for the Pt_nNDI_2 systems could reflect the fact that exciton transport occurs along the conjugated chain, where there is likely larger electronic coupling than between molecules in a disordered glassy solid. For electron transport in the Pt—acetylide chain the major, 59 ps component corresponds to a mobility μ = 0.067 cm^2/V-s ($D = 1.4 \times 10^{-3}$ cm^2/s, hopping time of τ = 3.6 ps), utilizing the relationship[26,82] between the diffusion coefficient and the principal exponential, which comprises 82% of the population.[26] The mobility obtained here is less than values reported for a poly(phenylene vinylene) and ladder-poly(phenylene)s by time-resolved microwave conductivity, where mobility in excess of 0.1 cm^2/V-s is observed,[22,23,79,83—85] but it is comparable to the electron mobility on poly(fluorene) chains determined by pulse radiolysis.[26]

SUMMARY AND CONCLUSION

This study has explored transport in relatively long conjugated oligomers containing organometallic complexes in the repeat unit structure. Using fast time-resolved pulse radiolysis and laser flash photolysis methods we have been able to directly probe the dynamics of electron and triplet exciton transport along the conjugated segments. The results show that transport of both carriers along these organometallic "molecular wires" is relatively rapid, occurring on time scales <200 ps over a distance of 3—5 nm. Analysis of the dynamics of charge and exciton transport suggests that the carriers move along the chain by an incoherent, site-to-site hopping mechanism, with hopping step times of ~27 ps per step for triplet excitons and <10 ps per step for negative polarons. The triplet hopping process may be gated by changes in the conformation of the monomers, with a tentative assignment to large amplitude torsional motion of phenylene units. Taken together the results provide insight into the mechanism of transport of carriers in organometallic conjugated electronic systems.

ASSOCIATED CONTENT

Supporting Information. Procedure for fitting pulse radiolysis data, additional pulse radiolysis transient absorption spectra and dynamics profiles, low-temperature emission spectra, and fit of pulse radiolysis dynamics to random-walk simulation. This material is available free of charge via the Internet at http://pubs.acs.org.

AUTHOR INFORMATION

Corresponding Author
jrmiller@bnl.gov (J.R.M.); kschanze@chem.ufl.edu (K.S.)

■ ACKNOWLEDGMENT

Work at the University of Florida was supported by the National Science Foundation (grant no. CHE-0515066). Pulse radiolysis studies were carried out at the Brookhaven National Laboratory with support from the Division of Chemical Sciences, Geosciences, and Biosciences, Office of Basic Energy Sciences of the U.S. Department of Energy through Grant DE-AC02-98-CH10886.

■ REFERENCES

(1) van Grondelle, R.; Novoderezhkin, V. I. *Phys. Chem. Chem. Phys.* **2006**, *8*, 793–807.
(2) Lee, H.; Cheng, Y. C.; Fleming, G. R. *Science* **2007**, *316*, 1462–1465.
(3) Holzwarth, A. R.; Muller, M. G.; Reus, M.; Nowaczyk, M.; Sander, J.; Rogner, M. *Proc. Natl. Acad. Sci. U.S.A.* **2006**, *103*, 6895–6900.
(4) Wasielewski, M. R.; Niemczyk, M. P.; Svec, W. A.; Pewitt, E. B. *J. Am. Chem. Soc.* **1985**, *107*, 1080–1082.
(5) Closs, G. L.; Miller, J. R. *Science* **1988**, *240*, 440–447.
(6) Wasielewski, M. R. *Chem. Rev.* **1992**, *92*, 435–461.
(7) Lewis, F. D.; Wu, T. F.; Zhang, Y. F.; Letsinger, R. L.; Greenfield, S. R.; Wasielewski, M. R. *Science* **1997**, *277*, 673–676.
(8) Lewis, F. D.; Letsinger, R. L.; Wasielewski, M. R. *Acc. Chem. Res.* **2001**, *34*, 159–170.
(9) Wasielewski, M. R. *J. Org. Chem.* **2006**, *71*, 5051–5066.
(10) Albinsson, B.; Martensson, J. *J. Photochem. Photobiol., C* **2008**, *9*, 138–155.
(11) Swager, T. M. *Acc. Chem. Res.* **1998**, *31*, 201–207.
(12) Davis, W. B.; Svec, W. A.; Ratner, M. A.; Wasielewski, M. R. *Nature* **1998**, *396*, 60–63.
(13) Creager, S.; Yu, C. J.; Bamdad, C.; O'Connor, S.; MacLean, T.; Lam, E.; Chong, Y.; Olsen, G. T.; Luo, J. Y.; Gozin, M.; Kayyem, J. F. *J. Am. Chem. Soc.* **1999**, *121*, 1059–1064.
(14) Weiss, E. A.; Wasielewski, M. R.; Ratner, M. A. In *Molecular Wires. From Design to Properties*; de Cola, L., Ed.; Springer: Berlin, 2005; pp 792−793.
(15) Reed, M. A.; Tour, J. M. *Sci. Am.* **2000**, *282*, 86–93.
(16) Tour, J. M. *Acc. Chem. Res.* **2000**, *33*, 791–804.
(17) Choi, S. H.; Kim, B.; Frisbie, C. D. *Science* **2008**, *320*, 1482–1486.
(18) Lafferentz, L.; Ample, F.; Yu, H.; Hecht, S.; Joachim, C.; Grill, L. *Science* **2009**, *323*, 1193–1197.
(19) Albinsson, B.; Eng, M. P.; Pettersson, K.; Winters, M. U. *Phys. Chem. Chem. Phys.* **2007**, *9*, 5847–5864.
(20) Swager, T. M.; Gil, C. J.; Wrighton, M. S. *J. Phys. Chem.* **1995**, *99*, 4886–4893.
(21) Beljonne, D.; Pourtois, G.; Silva, C.; Hennebicq, E.; Herz, L. M.; Friend, R. H.; Scholes, G. D.; Setayesh, S.; Mullen, K.; Bredas, J. L. *Proc. Natl. Acad. Sci. U.S.A.* **2002**, *99*, 10982–10987.
(22) Prins, P.; Grozema, F. C.; Schins, J. M.; Patil, S.; Scherf, U.; Siebbeles, L. D. A. *Phys. Rev. Lett.* **2006**, *96*, 146601.
(23) Prins, P.; Grozema, F. C.; Schins, J. M.; Savenije, T. J.; Patil, S.; Scherf, U.; Siebbeles, L. D. A. *Phys. Rev. B* **2006**, *73*, 045204.
(24) Funston, A. M.; Silverman, E. E.; Schanze, K. S.; Miller, J. R. *J. Phys. Chem. B* **2006**, *110*, 17736–17742.
(25) Asaoka, S.; Takeda, N.; Iyoda, T.; Cook, A. R.; Miller, J. R. *J. Am. Chem. Soc.* **2008**, *130*, 11912–11920.
(26) Shibano, Y.; Imahori, H.; Sreearunothai, P.; Cook, A. R.; Miller, J. R. *J. Phys. Chem. Lett.* **2010**, *1*, 1492–1496.
(27) Baldo, M. A.; Lamansky, S.; Burrows, P. E.; Thompson, M. E.; Forrest, S. R. *App. Phys. Lett.* **1999**, *75*, 4–6.
(28) Baldo, M. A.; O'Brien, D. F.; You, Y.; Shoustikov, A.; Sibley, S.; Thompson, M. E.; Forrest, S. R. *Nature* **1998**, *395*, 151–154.
(29) Guo, F. Q.; Kim, Y. G.; Reynolds, J. R.; Schanze, K. S. *Chem. Commun.* **2006**, 1887–1889.
(30) Mei, J.; Ogawa, K.; Kim, Y. G.; Heston, N. C.; Arenas, D. J.; Nasrollahi, Z.; McCarley, T. D.; Tanner, D. B.; Reynolds, J. R.; Schanze, K. S. *ACS Appl. Mater. Interfaces* **2009**, *1*, 150–161.
(31) Chawdhury, N.; Köhler, A.; Friend, R. H.; Younus, M.; Long, N. J.; Raithby, P. R.; Lewis, J. *Macromolecules* **1998**, *31*, 722–727.
(32) Chawdhury, N.; Köhler, A.; Friend, R. H.; Wong, W. Y.; Lewis, J.; Younus, M.; Raithby, P. R.; Corcoran, T. C.; Al-Mandhary, M. R. A.; Khan, M. S. *J. Chem. Phys.* **1999**, *110*, 4963–4970.
(33) Wilson, J. S.; Köhler, A.; Friend, R. H.; Al-Suti, M. K.; Al-Mandhary, M. R. A.; Khan, M. S.; Raithby, P. R. *J. Chem. Phys.* **2000**, *113*, 7627–7634.
(34) Wilson, J. S.; Chawdhury, N.; Al-Mandhary, M. R. A.; Younus, M.; Khan, M. S.; Raithby, P. R.; Köhler, A.; Friend, R. H. *J. Am. Chem. Soc.* **2001**, *123*, 9412–9417.
(35) Köhler, A.; Wilson, J. S.; Friend, R. H.; Al-Suti, M. K.; Khan, M. S.; Gerhard, A.; Bassler, H. *J. Chem. Phys.* **2002**, *116*, 9457–9463.
(36) Liu, Y.; Jiang, S. J.; Glusac, K.; Powell, D. H.; Anderson, D. F.; Schanze, K. S. *J. Am. Chem. Soc.* **2002**, *124*, 12412–12413.
(37) Haskins-Glusac, K.; Ghiviriga, I.; Abboud, K. A.; Schanze, K. S. *J. Phys. Chem. B* **2004**, *108*, 4969–4978.
(38) Silverman, E. E.; Cardolaccia, T.; Zhao, X. M.; Kim, K. Y.; Haskins-Glusac, K.; Schanze, K. S. *Coord. Chem. Rev.* **2005**, *249*, 1491–1500.
(39) Glusac, K.; Köse, M. E.; Jiang, H.; Schanze, K. S. *J. Phys. Chem. B* **2007**, *111*, 929–940.
(40) Wong, W. Y. *Dalton Trans.* **2007**, 4495–4510.
(41) Rogers, J. E.; Cooper, T. M.; Fleitz, P. A.; Glass, D. J.; McLean, D. G. *J. Phys. Chem. A* **2002**, *106*, 10108–10115.
(42) Wilson, J. S.; Dhoot, A. S.; Seeley, A.; Khan, M. S.; Köhler, A.; Friend, R. H. *Nature* **2001**, *413*, 828–831.
(43) Zhou, G.; He, Y.; Yao, B.; Dang, J. S.; Wong, W.-Y.; Xie, Z.; Zhao, X.; Wang, L. *Chem. Asian J.* **2010**, *5*, 2405–2414.
(44) Wong, W. Y.; Ho, C. L. *Acc. Chem. Res.* **2010**, *43*, 1246–1256.
(45) Rogers, J. E.; Slagle, J. E.; Krein, D. M.; Burke, A. R.; Hall, B. C.; Fratini, A.; McLean, D. G.; Fleitz, P. A.; Cooper, T. M.; Drobizhev, M.; Makarov, N. S.; Rebane, A.; Kim, K. Y.; Farley, R.; Schanze, K. S. *Inorg. Chem.* **2007**, *46*, 6483–6494.
(46) Kim, K. Y.; Shelton, A. H.; Drobizhev, M.; Makarov, N.; Rebane, A.; Schanze, K. S. *J. Phys. Chem. A* **2010**, *114*, 7003–7013.
(47) Zhou, G. J.; Wong, W. Y.; Poon, S. Y.; Ye, C.; Lin, Z. Y. *Adv. Funct. Mater.* **2009**, *19*, 531–544.
(48) Cardolaccia, T.; Funston, A. M.; Köse, M. E.; Keller, J. M.; Miller, J. R.; Schanze, K. S. *J. Phys. Chem. B* **2007**, *111*, 10871–10880.
(49) Haskins-Glusac, K.; Pinto, M. R.; Tan, C. Y.; Schanze, K. S. *J. Am. Chem. Soc.* **2004**, *126*, 14964–14971.
(50) Devi, L. S.; Al-Suti, M. K.; Dosche, C.; Khan, M. S.; Friend, R. H.; Köhler, A. *Phys. Rev. B* **2008**, *78*, 045210.
(51) Schull, T. L.; Kushmerick, J. G.; Patterson, C. H.; George, C.; Moore, M. H.; Pollack, S. K.; Shashidhar, R. *J. Am. Chem. Soc.* **2003**, *125*, 3202–3203.
(52) Keller, J. M.; Schanze, K. S. *Organometallics* **2009**, *28*, 4210–4216.
(53) Demas, J. N.; Crosby, G. A. *J. Phys. Chem.* **1971**, *75*, 991–1024.
(54) Accelerators for Ultrafast Phenomena. In *Radiation Chemistry: Present Status and Future Trends*; Wishart, J. F., Ed.; Elsevier Science: New York, 2001; Vol. 87.
(55) Wishart, J. F.; Cook, A. R.; Miller, J. R. *Rev. Sci. Instrum.* **2004**, *75*, 4359–4366.
(56) Miller, J. R.; Penfield, K.; Johnson, M.; Closs, G.; Green, N. *Adv. Chem. Ser.* **1998**, *254*, 161–176.
(57) Funston, A. M.; Silverman, E. E.; Miller, J. R.; Schanze, K. S. *J. Phys. Chem. B* **2004**, *108*, 1544–1555.
(58) Takeda, N.; Asaoka, S.; Miller, J. R. *J. Am. Chem. Soc.* **2006**, *128*, 16073–16082.
(59) De Waele, V.; Sorgues, S.; Pernot, P.; Marignier, J. L.; Monard, H.; Larbre, J. P.; Mostafavi, M. *Chem. Phys. Lett.* **2006**, *423*, 30–34.
(60) De Waele, V.; Sorgues, S.; Pernot, P.; Marignier, J. L.; Mostafavi, M. *Nucl. Sci. Techn.* **2007**, *18*, 10–15.

(61) Glinec, Y.; Faure, J.; Guemnie-Tafo, A.; Malka, V.; Monard, H.; Larbre, J. P.; De Waele, V.; Marignier, J. L.; Mostafavi, M. *Rev. Sci. Instrum.* **2006**, *77*.
(62) Cook, A. R.; Shen, Y. *Rev. Sci. Instrum.* **2009**, *80*, 073106.
(63) Tranthi, T. H.; Koulkes-Pujo, A. M. *J. Phys. Chem.* **1983**, *87*, 1166–1169.
(64) Danilov, E. O.; Pomestchenko, I. E.; Kinayyigit, S.; Gentili, P. L.; Hissler, M.; Ziessel, R.; Castellano, F. N. *J. Phys. Chem. A* **2005**, *109*, 2465–2471.
(65) Frapper, G.; Kertesz, M. *Inorg. Chem.* **1993**, *32*, 732–740.
(66) Greenfield, S. R.; Svec, W. A.; Gosztola, D.; Wasielewski, M. R. *J. Am. Chem. Soc.* **1996**, *118*, 6767–6777.
(67) Ramakrishna, G.; Goodson, T.; Rogers-Haley, J. E.; Cooper, T. M.; McLean, D. G.; Urbas, A. *J. Phys. Chem. C* **2009**, *113*, 1060–1066.
(68) The latter term in this expression is the Coulombic stabilization energy in the charge-separated state. Assuming a charge separation distance of 1 nm in THF solution this term is −0.19 eV. This indicates that the electron−hole pair is strongly bound in the charge-separated state, and therefore, it is unlikely that the hole is able to diffuse into the center of the Pt−acetylide chain in the longer oligomers.
(69) Oevering, H.; Paddon Row, M. N.; Heppener, M.; Oliver, A. M.; Cotsaris, E.; Verhoeven, J. W.; Hush, N. S. *J. Am. Chem. Soc.* **1987**, *109*, 3258–3269.
(70) Sreearunothai, P.; Asaoka, S.; Cook, A. R.; Miller, J. R. *J. Phys. Chem. A* **2009**, *113*, 2786–2795.
(71) It would be desirable to monitor the 475 nm absorption due to $NDI^{\bullet-}$ in order to observe fast appearance of electrons at the NDI end groups. However, measurement at 475 nm is difficult because the intense absorption of ground state neutral $Pt_{10}NDI_2$ molecules at the high concentration needed to capture electrons reduces the analyzing light intensity by a factor of ∼100. In addition, the OFSS instrument is not yet able to operate effectively at 475 nm. A measurement at 480 nm with a biplanar phototube detector (150 ps nominal resolution) is shown in Figure S-3 (Supporting Information).
(72) Gaines, G. L.; Oneil, M. P.; Svec, W. A.; Niemczyk, M. P.; Wasielewski, M. R. *J. Am. Chem. Soc.* **1991**, *113*, 719–721.
(73) At longer times the transient absorption at 478 nm decays, presumably due to relaxation of the charge-separated state via charge recombination.
(74) Closs, G. L.; Johnson, M. D.; Miller, J. R.; Piotrowiak, P. *J. Am. Chem. Soc.* **1989**, *111*, 3751–3753.
(75) Hoffmann, S. T.; Bässler, H.; Koenen, J. M.; Forster, M.; Scherf, U.; Scheler, E.; Strohriegl, P.; Köhler, A. *Phys. Rev. B* **2010**, *81*, 115103.
(76) Hoffmann, S. T.; Scheler, E.; Koenen, J. M.; Forster, M.; Scherf, U.; Strohriegl, P.; Bässler, H.; Köhler, A. *Phys. Rev. B* **2010**, *81*, 165208.
(77) Pejov, L.; La Rosa, M.; Kocarev, L. *Chem. Phys.* **2007**, *340*, 1–11.
(78) McLendon, G.; Pardue, K.; Bak, P. *J. Am. Chem. Soc.* **1987**, *109*, 7540–7541.
(79) Hoofman, R. J. O. M.; De Haas, M. P.; Siebbeles, L. D. A.; Warman, J. M. *Nature (London)* **1998**, *392*, 54–56.
(80) Giebink, N. C.; Sun, Y.; Forrest, S. R. *Org. Electron.* **2006**, *7*, 375–386.
(81) Namdas, E. B.; Ruseckas, A.; Samuel, I. D. W.; Lo, S. C.; Burn, P. L. *App. Phys. Lett.* **2005**, *86*, 3.
(82) Carslaw, H. S.; Jaeger, J. C. *Conduction of Heat in Solids*, 2nd ed.; Oxford University Press, New York, 1986.
(83) Grozema, F. C.; Warman, J. M. *Radiat. Phys. Chem.* **2005**, *74*, 234–238.
(84) Devizis, A.; Serbenta, A.; Meerholz, K.; Hertel, D.; Gulbinas, V. *Phys. Rev. Lett.* **2009**, *103*, 027404.
(85) Devizis, A.; Meerholz, K.; Hertel, D.; Gulbinas, V. *Phys. Rev. B* **2010**, *82*, 155204 1–8.